Supplemental material to this article can be found at:
http://molpharm.aspetjournals.org/content/suppl/2021/05/07/molpharm.121.000266.DC1
1521-0111/100/1/46–56$35.00 https://doi.org/10.1124/molpharm.121.000266
MOLECULAR PHARMACOLOGY Mol Pharmacol 100:46–56, July 2021

Molecular Determinants Underlying Delta Selective Compound 2 Activity at δ-Containing $GABA_A$ Receptors[S]

Christina B. Falk-Petersen, Frederik Rostrup, Rebekka Löffler, Stine Buchleithner, Kasper Harpsøe, David E. Gloriam, Bente Frølund, and Petrine Wellendorph

Department of Drug Design and Pharmacology, Faculty of Health and Medical Sciences, University of Copenhagen, Copenhagen, Denmark

Received February 18, 2021; accepted April 22, 2021

ABSTRACT

Delta selective compound 2 (DS2; 4-chloro-*N*-[2-(2-thienyl)imidazo[1,2-*a*]pyridin-3-yl]benzamide) is one of the most widely used tools to study selective actions mediated by δ-subunit–containing $GABA_A$ receptors. DS2 was discovered over 10 years ago, but despite great efforts, the precise molecular site of action has remained elusive. Using a combination of computational modeling, site-directed mutagenesis, and cell-based pharmacological assays, we probed three potential binding sites for DS2 and analogs at $\alpha_4\beta_1\delta$ receptors: an $\alpha_4^{(+)}\delta^{(-)}$ interface site in the extracellular domain (ECD), equivalent to the diazepam binding site in $\alpha\beta\gamma_2$ receptors, and two sites in the transmembrane domain (TMD) - one in the $\alpha_4^{(+)}\beta_1^{(-)}$ and one in the $\alpha_4^{(-)}\beta_1^{(+)}$ interface, with the $\alpha_4^{(-)}\beta_1^{(+)}$ site corresponding to the binding site for etomidate and a recently disclosed low-affinity binding site for diazepam. We show that mutations in the ECD site did not abrogate DS2 modulation. However, mutations in the TMD $\alpha_4^{(+)}\beta_1^{(-)}$ interface, either α_4(S303L) of the $\alpha_4^{(+)}$ side or β_1(I289Q) of the $\beta_1^{(-)}$ side, convincingly disrupted the positive allosteric modulation by DS2. This was consistently demonstrated both in an assay measuring membrane potential changes and by whole-cell patch-clamp electrophysiology and rationalized by docking studies. Importantly, general sensitivity to modulators was not compromised in the mutated receptors. This study sheds important light on the long-sought molecular recognition site for DS2, refutes the misconception that the selectivity of DS2 for δ-containing receptors is caused by a direct interaction with the δ-subunit, and instead points toward a functional selectivity of DS2 and its analogs via a surprisingly well conserved binding pocket in the TMD.

SIGNIFICANCE STATEMENT

δ-Containing $GABA_A$ receptors represent potential drug targets for the treatment of several neurological conditions with aberrant tonic inhibition, yet no drugs are currently in clinical use. With the identification of the molecular determinants responsible for positive modulation by the known compound delta selective compound 2, the ground is laid for design of ligands that selectively target δ-containing $GABA_A$ receptor subtypes, for better understanding of tonic inhibition, and ultimately, for rational development of novel drugs.

Introduction

Inhibition in the brain is primarily mediated by GABA acting through GABA receptors, with the ionotropic GABA type A receptors ($GABA_AR$) being responsible for fast inhibition. Thus, $GABA_ARs$ play an essential role in transmitting inhibitory signaling in the brain. Structurally speaking, $GABA_ARs$ belong to the Cys-loop receptor family of pentameric receptor complexes and are composed from a repertoire of 19 different subunits in mammals, with the most commonly expressed in the central nervous system being $\alpha_{1\text{-}6}$, $\beta_{1\text{-}3}$, $\gamma_{1\text{-}3}$, and δ (Olsen and Sieghart, 2009). The subunit stoichiometry of the archetypical $GABA_A$ receptor is 2α, 2β, and a third subunit, most typically a γ- or a δ-subunit, but other stoichiometries have also been reported (Olsen and Sieghart, 2009). Studies on the subunit arrangement of the most abundantly expressed synaptic subtype, $\alpha_1\beta_2\gamma_2$, and a number of other γ-containing subtypes, show that the subunits are arranged as γ-β-α-β-α in a counterclockwise fashion around the central ion channel (Tretter et al., 1997; Baumann et al., 2002). Although it is generally accepted that the δ-subunit in its cognate receptors simply replaces the γ-subunit with respect to arrangement (Barrera et al., 2008), this is still not unequivocally established (Baur et al., 2009; Kaur et al., 2009; Wagoner and Czajkowski, 2010; Patel et al., 2014). Irrespectively, the

This work was financially supported by the Lundbeck Foundation [Grant R230-2016-2562] (to C.B.F-P.) and [Grant R277-2018-260] (to P.W.) and the Drug Research Academy (C.B.F-P. and F.R.). F.R was financially supported by a 2018 Lundbeck Foundation pregraduate scholar stipend in pharmaceutical neuroscience.

The authors declare no conflict of interest.

Part of this work was described in the Ph.D. thesis by C.B.F.-P.: Falk-Petersen CB (2020) *Pharmacological insight into $GABA_A$ receptors with focus on β_1-containing extrasynaptic subtypes* Ph.D. thesis, the Faculty of Health and Medical Sciences, University of Copenhagen, Denmark.

https://doi.org/10.1124/molpharm.121.000266.

[S] This article has supplemental material available at molpharm.aspetjournals.org.

ABBREVIATIONS: Br-DS2OPh, *N*-(6-bromo-2-(thiophen-2-yl)imidazo[1,2-*a*]pyridin-3-yl)-4-phenoxybenzamide; cryo-EM, cryogenic electron microscopy; DS2, delta selective compound 2; DS2OMe, (4-methoxy-*N*-[2-(thiopen-2-yl)imidazole[1,2-*a*]pyridine-3-yl]benbamide); ECD, extracellular domain; FMP, fluorometric imaging plate reader membrane potential; $GABA_AR$, GABA type A receptor; HEK, human embryonic kidney; PAM, positive allosteric modulator; RFU, relative fluorescence unit; TMD, transmembrane domain; WT, wild type.

orthosteric binding sites are located at the $\beta^{(+)}\alpha^{(-)}$ interfaces in the extracellular domain (ECD), and a number of allosteric binding sites have also been identified in the subunit interfaces of both the ECD and TMD (Olsen, 2018). These include, for example, the benzodiazepine site in the ECD $\alpha^{(+)}\gamma^{(-)}$ interface, responsible for mediating the anxiolytic and sleep-inducing effect of the benzodiazepines, including diazepam (Valium), widely used in the clinic (Sigel and Steinmann, 2012; Simeone et al., 2019).

The δ-containing $GABA_A$Rs are located primarily at extrasynaptic sites where they mediate tonic (persistent) inhibition (Mody, 2001; Farrant and Nusser, 2005), hence controlling neuronal excitability (Belelli et al., 2009). Tonic inhibition is involved in various physiologic responses and pathophysiological conditions (Lee and Maguire, 2014), underlining a continued interest in targeting these receptors in conditions like insomnia (Wafford and Ebert, 2006), ischemic stroke (Clarkson et al., 2010; Lie et al., 2019), some forms of epilepsy (Cope et al., 2009), and peripheral immunomodulation (Yocum et al., 2017; Neumann et al., 2019). However, compared with the synaptic γ-containing receptors, pronounced insight into the physiologic and pathophysiological role of δ-containing receptors is still limited by the low number of potent and selective compounds.

One highly used model compound with selectivity for δ-containing receptors is the positive allosteric modulator (PAM) delta selective compound 2 (DS2; 4-chloro-*N*-[2-(2-thienyl)imidazo[1,2-*a*]pyridin-3-yl]benzamide) (Wafford et al., 2009). DS2 is extensively used as a tool compound to confirm the presence of δ-receptor–mediated tonic currents both in vitro and in vivo (Wongsamitkul et al., 2016; Falk-Petersen et al., 2017; Zhang et al., 2017; Dalby et al., 2020). DS2 was identified in a screening campaign and reported as a δ-selective PAM at $\alpha_4\beta_3\delta$ $GABA_A$Rs, showing no or limited effects at $\alpha_4\beta_3\gamma_2$ and $\alpha_1\beta_3\gamma_2$ receptors (Wafford et al., 2009). This selectivity was confirmed in thalamic relay neurons, where only extrasynaptic tonic currents were enhanced (Wafford et al., 2009), and using $\delta^{-/-}$ mice (Jensen et al., 2013). DS2 displays limited brain permeability (Jensen et al., 2013) but was, nonetheless, shown to improve recovery after stroke in mice, plausibly by dampening peripheral immune activation (Neumann et al., 2019). Recently, a methoxy analog of DS2, termed DS2OMe, was identified and confirmed to have potential as a positron emission tomography tracer for visualization of δ-containing receptors in brains of larger mammals, such as pig (L'Estrade et al., 2019).

In 2018, the first cryogenic electron microscopy (cryo-EM) structure of a human $GABA_A$R pentamer $\alpha_1\beta_2\gamma_2$ was published (Zhu et al., 2018). Afterward, a structure of the $\alpha_1\beta_3\gamma_2$ receptor was solved in complex with diazepam, revealing both the known high-affinity diazepam binding site in the $\alpha^{(+)}\gamma^{(-)}$ interface in the ECD and a novel low-affinity binding site located in the $\alpha^{(-)}\beta^{(+)}$ interface of the TMD (Masiulis et al., 2019).

Based on the notion that binding pockets evolved through nature are often highly conserved, combined with the structural similarities between DS2 and the benzodiazepine site ligand zolpidem (Rostrup et al., 2021), we hypothesized that similar pockets are present in δ-containing subtypes and that either of them could represent the long-sought-after DS2 site. We here report the identification of two residues, α_4(S303) and β_1(I289), within the predicted $\alpha_4{}^{(+)}\beta_1{}^{(-)}$ TMD interface of $\alpha_4\beta_1\delta$ receptors as necessary for DS2 modulation. These findings are supported by docking of DS2 analogs into the identified binding pocket.

Materials and Methods

General. The study is exploratory by nature and follows the guidelines detailed in Michel et al. (2020). Data collection were in some cases defined by some preset standards, as detailed under each experimental section.

Chemicals and Materials. The compounds DS2, (4-chloro-N-[2-(2-thienyl)imidazo[1,2-a]pyridin-3-yl]benzamide); AA29504, ([2-amino-4-(2,4,6-trimethylbenzylamino)-phenyl]-carbamic acid ethyl ester); etomidate, ((*R*)-1-(1- phenylethyl)-1H-imidazole-5-carboxylic acid ethyl ester); picrotoxin; and GABA were obtained from Tocris Bioscience (Bristol, UK). DS2OMe (4-methoxy-*N*-[2-(thiopen-2-yl)imidazole[1,2-*a*]pyridine-3-yl]benbamide) was synthesized in-house as described previously (Yakoub et al., 2018). The purity test was done by High Performance Liquid Chromatography (HPLC), and the combustion analysis calculated for $C_{19}H_{15}N_3O_2S$ was 350.09 and was found to be 350.09. Reverse-phase High Performance Liquid Chromatography (HPLC) is as follows: Retention time (MeCN/H_2O, 1:1) = 6.75 minutes, purity > 99%. DMEM with GlutaMAX-I, FBS, penicillin-streptomycin, hygromycin B, trypsin-EDTA, Dulbecco's phosphate-buffered saline, and Hank's balanced salt solution were purchased from Life Technologies (Paisley, UK). DMSO, HEPES, $MgCl_2$, $CaCl_2$, polyd-lysine, and MgATP were purchased from Sigma-Aldrich (St. Louis, MO). The fluorometric imaging plate reader membrane potential (FMP) Blue dye was purchased from Molecular Devices (Crawley, UK), and Polyfect transfection reagent was from Qiagen (West Sussex, UK). Stocks of DS2 and DS2OMe were prepared at 1 mM and 10 mM concentrations in DMSO with final DMSO concentration < 0.1%. Because of the moderate solubility and 4× concentrations used in the FMP assay, the buffer was preheated to 37°C in a water bath before addition of compound and preparation of serial dilutions. Only stocks with final concentrations below 12 μM were used for further dilutions. Furthermore, higher concentrations were prepared separately.

Cells and Transfections. A human embryonic kidney (HEK) 293 Flp-In cell line stably expressing the human δ-$GABA_A$R subunit (Falk-Petersen et al., 2017) was used for transfection, with human α- and β-subunits to express recombinant wild-type (WT) and mutant $GABA_A$Rs, using transfection ratios optimized as described (Falk-Petersen et al., 2017). Cells were maintained in DMEM containing GlutaMAX-I supplemented with 10% FBS and 1% penicillin-streptomycin and kept in an incubator at 37°C and a humidity of 5% CO_2. In total, 200 μl/ml hygromycin B was added to the media as positive selection. Transfection was performed using Polyfect (Qiagen) following the manufacturer's instructions, except for using half the volume of transfection reagent for each transfection. The α- and β-subunits were cotransfected in a 1:1 ratio for FMP experiments and, for patch-clamp experiments, additionally cotransfected with GFP in a 0.5:1:1 ratio (0.8:1.6:1.6 μg in 6-cm culture dishes) to visualize transfected cells.

Plasmids and Mutant Constructs. The plasmids used for transfection to transiently express $GABA_A$ receptors have been described previously (Falk-Petersen et al., 2017). The WT human α_4- and β_1-subunits were subcloned into the pUNIV vector (Addgene, Cambridge, MA) and the human δ-subunit into the pcDNA5/FRT vector (Invitrogen, Paisley, UK) using the δ-construct described previously (Falk-Petersen et al., 2017). Plasmids carrying single and double mutations were generated and sequence-verified by GenScript (Piscataway, NJ). The numbering of the mutants refers to the sequences with the signal peptide included.

Generation of Stable Cell Lines. Mutations introduced into the δ-subunit were established as stable HEK293 Flp-In cell lines (Invitrogen), generating a stable cell line for each mutant. The stable cell lines were generated using the pcDNA/FRT/V5-His TOPO TA Expression kit (Invitrogen) performed according to the manufacturer's protocol and as described previously (Falk-Petersen et al.,

2017), except for using 25 μl Polyfect and 4 μg DNA for transfection in a 10-cm culture dish.

Fluorometric Imaging Plate Reader Membrane Potential Assay. The FMP assay was performed exactly as described previously (Falk-Petersen et al., 2017). In brief, 48 hours before the assay, cells were transfected. At 16–20 hours later, cells were plated into clear-bottomed poly(D-lysine)–coated black 96-well plates in a number of 50,000 cells per well, suspended in cell media, and placed in an incubator at 37°C with a humidity of 5% CO_2 until performing the assay. At 44–48 hours post-transfection, the medium was removed, and cells were washed in assay buffer (100 μl/well) and incubated in 100 μl/well 0.5 mg/ml FMP Blue dye freshly dissolved in assay buffer (Hank's balanced salt solution containing 20 mM HEPES adjusted to pH 7.4 and supplemented with 2 mM $CaCl_2$ and 0.5 mM $MgCl_2$) for 30 minutes and shielded from light in an incubator at 37°C and a humidity of 5% CO_2. Ligand solutions were prepared in 4× assay buffer and added to a ligand plate, which was placed in a FLEXstation3 plate reader (Molecular Devices, Crawley, UK) that was preheated to 37°C for temperature equilibration for 10–15 minutes. After transferring the cell plate to the reader, the fluorescence was measured at baseline and after ligand addition by detecting emission at 560 nm caused by excitation at 530 nm.

FMP Experimental Design and Data Analysis. For FMP experiments, some preset formats were used for assay design and data analysis. Compound-induced signals were reported as changes in relative fluorescence units (ΔRFU), with the signal given as the difference between the average of the baseline signal (~30-second recording) subtracted the peak response (or minimum response for decreases in baseline). All raw traces were manually inspected for obvious artifacts after compound addition. For high concentrations of DS2 (1–20 μM), we regularly observed negative RFU values below the buffer responses that in certain cases were excluded (see below). This phenomenon was independent of receptor subtype, as it was observed for both δ-HEK and mock cells. The phenomenon was less pronounced for DS2OMe, which is why this compound was preferred in some substudies. To circumvent this problem, we set up the following exclusion criteria: negative ΔRFU or decreased ΔRFU values for high concentration (>1 μM) of DS2 and DS2OMe compared with the ΔRFU for a lower concentration in the same experiment (indicative of precipitation). Additionally, curve fittings resulting in ambiguous EC_{50} values and R^2 values lower than 0.80 due to very small responses were omitted from analyses, resulting in the following number of excluded experiments (excluded/total number) using either DS2 or DS2OMe at the given receptor subtypes: $\alpha_4\beta_1\delta$, 6/18; α_4(F133A), 2/7; α_4(F133L), 4/7; α_4(R135A), 6/10; α_4(R135H), 4/7; α_4(G191A), 4/8; α_4(G191E), 2/7; α_4(G191L), 4/7; δ(E71L), 0/5; δ(F90A), 0/4; δ(H204A), 1/5; δ(S155Q), 1/5; δ(A73N), 1/5; α_4(S303L), 0/3; α_4(L302Y), 1/5; α_4(L302Y,S303L), 2/5; β_1(I289Q), 1/8; β_1(S290F), 0/4. For mutants, experiments were generally performed in three to five independent experiments with technical triplicates, which was decided prior to execution based on the level of variation observed in previous work. For technical reasons, a few experiments had to be conducted at $n = 6$ to 7 (Supplemental Table 5; Table 1). WT data were performed in 8–11 independent experiments, as they served as controls across experiments.

Experimental data are shown in scatter plots with 95% confidence intervals with n values given in the figure legends. Curves were normalized to GABA to allow side-by-side representation and depicted as representative data (means ± S.D.). Mean EC_{50} values and pEC_{50} values with 95% confidence intervals are collected in tables along with statistical values. Concentration-response curves were fitted using nonlinear regression, with log-transformed concentrations as x-values, using the four-parameter concentration-response equation,

$$Response = bottom + \frac{top - bottom}{1 + 10^{[(logEC_{50} - x)\cdot n_H]}},$$

to determine the EC_{50} value and Hill slope (n_H). The "bottom" and "top" denote the upper and lower nonconstrained plateau of the curve, respectively. The calculated EC_{50} values were log-transformed to obtain mean pEC_{50} values. Statistical analysis of mutated receptors was performed on the pEC_{50} values using the two-sided Welch's t test compared with WT, correcting for multiple comparison using the original FDR method of Benjamini and Hochberg with a discovery rate of 0.05. Both adjusted and unadjusted P values are reported. Data analysis and statistics were performed in GraphPad Prism (version 8.4.3; GraphPad, San Diego, CA).

Whole-Cell Patch-Clamp Electrophysiology. Whole-cell patch-clamp experiments were performed on δ-HEK cells transiently coexpressing WT or mutant α- and β-subunits and GFP as described previously (Falk-Petersen et al., 2020). In short, the transfected cells were transferred to 35-mm Petri dishes (100,000–200,000 cells) the day prior to performing the experiment. On the day of experiment, cell media were exchanged for ABSS [containing the following (in mM): NaCl 140, KCl 3.5, Na_2HPO_4 1.25, $MgSO_4$ 2, $CaCl_2$ 2, glucose 10, and HEPES 10; pH 7.35] at room temperature (20–24°C) before placing at the stage of an Axiovert 10 microscope (Zeiss, Germany). Viewing the cells at 200× magnification and visualizing cells containing green fluorescent protein with UV light from an HBO 50 lamp (Zeiss, Germany), the cells were approached with micropipettes of 1.2–3.3 MΩ resistance manufactured from 1.5-mm OD glass (World Precision Instruments, Sarasota, FL) on a microelectrode puller, model PP-830 (Narishige, Tokyo, Japan). The micropipettes contained an intracellular solution composed of the following (in mM): KCl 140, $MgCl_2$ 1, $CaCl_2$ 1, EGTA 10, MgATP 2, and HEPES 10; pH 7.3.

Recordings were made from cells in the whole-cell configuration using the standard patch-clamp technique in voltage mode and an EPC-9 amplifier (HEKA, Lambrecht, Germany). The clamping potential was −60 mv, and series resistance was 80% compensated. Whole-cell currents were recorded using Pulse and PulseFit software (version 8.80; HEKA). Ligand solutions, prepared in ABSS, were applied using two VC3-8xP pressurized application systems feeding into a 16-barreled perfusion pipette (ALA Scientific Instruments Inc., Farmingdale, NY) ending approximately 100 μm from the recorded cell. PAMs were tested using coapplication with a concentration of GABA corresponding to GABA $EC_{10–35}$ at the respective receptor subtype. Preapplication was not used for DS2 and DS2OMe, as results from preliminary experiments showed no difference in the size of the peak current with and without preapplication of the PAM. PAMs and GABA were coapplied for 10–30 seconds until the peak current was reached. Agonists were applied for 5 seconds. Between compound applications, compound-free ABSS was applied from one of the barrels to quickly remove the compounds from the cell, and cells were allowed to recover for 1 minute before the next ligand application.

Patch-Clamp Data Analysis and Statistics. As for FMP, some preset formats regarding assay design and data analysis were used. All currents were normalized to the maximum GABA current and given as $\%I/I_{max}$. All currents are reported as normalized mean currents with 95% confidence interval. Based on previous experience, currents from at least five different cells from at least two transfections were used. In a few cases, up to 16 cells were used for technical reasons (see Supplemental Fig. 4). All n values are given in the figure legends. Data sets with GABA controls (0.1–0.5 μM) deviating from GABA EC_{10} to EC_{35} were excluded from the analysis.

Statistical analysis was applied to test whether the PAMs potentiated the GABA control response using two-sided Welch's t test as for FMP data. Analysis of currents was performed using Pulse and PulseFit (HEKA), and current traces were visualized using IgorPro (version 6.2.2.2; Wavemetrics, Lake Oswego, OR). Collected data and statistical analysis were performed using GraphPad Prism (version 8.4.3).

Homology Model for the Extracellular Domain Binding Site. The homology model of the ECD $\alpha_4^{(+)}\beta_1^{(-)}$ interface has been described previously (Rostrup et al., 2021). The model was used to identify residues for the mutational study based on the docking of DS2 into the model described previously (Rostrup et al., 2021).

Homology Model for the Transmembrane Domain Binding Site. The homology model of the transmembrane part of the $\alpha_4\beta_1$ interface was constructed with Modeler 9.24 (Webb and Sali, 2016) using the $\alpha_1\beta_3$ interface from the $\alpha_1\beta_3\gamma_{2L}$ crystal structure (Protein Data Bank code: 6HUP) (Masiulis et al., 2019) as template. Model and template sequences of the transmembrane helices and the connecting loops making up the subunit interface were obtained and aligned in UniProt (http://www.uniprot.org/) (UniProt Consortium, 2019): sequence IDsα_4 P48169, β_1 P18505, α_1 P114867, and β_3 P28472. To adhere as much as possible to the very closely related template structure, the "very fast" keyword was used to output the initial model that is only subjected to a brief optimization, thus retaining the copied coordinates for all conserved residue positions. This procedure was selected based on the high sequence similarities and assumed structural conservation combined with the fact that the binding site residues are optimized relative to the ligand in following computational steps.

Induced-Fit Docking of DS2 into the Transmembrane $\alpha_4^{(+)}\beta_1^{(-)}$ Site and In Silico Mutagenesis. The homology models were prepared for docking with the Protein Preparation Wizard [Schrödinger Release 2020-2; Schrödinger, LLC, New York, NY (Sastry et al., 2013)] using default settings. The chemical structure of DS2 was downloaded from the PubChem database (https://pubchem.ncbi.nlm.nih.gov) (Kim et al., 2019; chemical ID: 979718), and the analogs DS2OMe (L'Estrade et al., 2019) and Br-DS2OPh (Rostrup et al., 2021) were built from DS2 in MarvinSketch 20.15.0 (ChemAxon; http://www.chemaxon.com). All three ligands were prepared for docking with default settings in LigPrep (Schrödinger Release 2020-2) and used for induced-fit docking in the model of the transmembrane $\alpha_4\beta_1$ interface with the standard protocol. The binding site center was defined by Ser303 and Ala324 from α_4 plus Pro253 and Ile289 from β_1. The ligand length was set to ≦14 Å, and XP precision was used in the redocking step, while all other settings were default. The best-scoring docking poses according to the IFD score were selected for each compound as the most likely binding mode. In silico mutagenesis was performed with the built-in protein mutagenesis wizard in PyMOL (The PyMOL Molecular Graphics System, version 2.0; Schrödinger, LLC.) and the backbone dependent rotamer library selecting the most probable rotamer with the fewest steric clashes with surrounding residues. For the α_4S303L and β_1I289Q mutations the first (one of four; 47.4%) and second (2 of 16, 14.6%) most likely rotamers were selected, respectively.

Results

To identify central residues for the activity of DS2 at δ-containing $GABA_ARs$, we systematically investigated three potential binding pockets: one in the ECD (the $\alpha_4^{(+)}\delta^{(-)}$ interface) and two in the TMD (the $\alpha_4^{(+)}\beta_1^{(-)}$ and the $\beta_1^{(+)}\alpha_4^{(-)}$ interfaces). Although δ-containing TMD interfaces are present in the receptor complex, we focused solely on the α-β interfaces because of the confirmed existence of binding sites at these interfaces (Ernst et al., 2005; Puthenkalam et al., 2016; Laverty et al., 2019) and our focus on benzodiazepine binding sites as potential binding sites for DS2 due to the structural resemblance between DS2 and zolpidem (Rostrup et al., 2021). Key interacting residues were identified using homology models and pharmacologically characterized in well established HEK cell–based assays using the $\alpha_4\beta_1\delta$ receptor as a model receptor, which has been carefully characterized in our hands (Falk-Petersen et al., 2017, 2020; Dalby et al., 2020).

Investigation of the ECD $\alpha^{(+)}\delta^{(-)}$ Interface as the Site of Modulation by DS2. First, using the homology model published in Rostrup et al. (2021), we studied the pocket located in the C-loop of the $\alpha^{(+)}\delta^{(-)}$ interface in the ECD of $\alpha_4\beta_1\delta$ receptors (Fig. 1A). From our previous docking into the model, we identified three potential key residues on the $\alpha_4^{(+)}$ side of the interface that could either interact directly with DS2 or were placed centrally within the binding pocket: α_4(F133), α_4(R135), and α_4(G191) (Fig. 1A). Additionally, five residues on the complementary $\delta^{(-)}$ interface were identified: δ(E71), δ(A73), δ(F90), δ(S155), and δ(H204). The selected residues were mutated with the principle of removing potential interactions (mutation into alanine) and/or gradually decreasing the space in the binding pocket (mutation into various amino acid residues), thus expecting a reduced modulation by DS2 compared with WT. This resulted in seven different α_4-subunit mutants and five different δ-subunit mutants (Supplemental Tables 1 and 2). Each of the mutated subunits were expressed in HEK cell lines to form $\alpha_4\beta_1\delta$ receptors and tested in the FMP assay as single mutants. Whereas α_4-mutants were simply cotransfected with WT β_1 into WT stable δ-HEK293 Flp-In cells, each of the δ-mutants were established as stable HEK293 Flp-In cell lines transfected with WT $\alpha_4\beta_1$ to transiently express $\alpha_4\beta_1\delta$. In general, extending the utility of this expression system from WT to mutated δ-containing receptors is highly reliable and suitable for controlling expression and reliably studying these in-some-instances cumbersome receptor subtypes (Karim et al., 2012).

All seven α_4-mutant receptors were found to express functionally active receptors and to respond to GABA with 2 to 3 times the potency observed for WT (Fig. 1, B and C; Supplemental Fig. 1; Supplemental Table 1). The expression levels of α_4(F133A/L)$\beta_1\delta$ and α_4(G191E)$\beta_1\delta$ appeared lower as compared with WT, as the maximal ΔRFU values were consistently reduced in all experiments (Fig. 1B). To characterize the sensitivity to DS2, it was applied together with a GABA EC_{20} concentration, calculated for each mutant (Supplemental Table 2; Table 1). Among the seven different α_4-mutants, α_4(F133A)$\beta_1\delta$ and α_4(G191E)$\beta_1\delta$ showed no apparent or only small modulation by DS2, whereas the potency of DS2 at the other α_4-subunit mutants was either unchanged [α_4(F133L)$\beta_1\delta$, α_4(R135A), and α_4(G191A/L)$\beta_1\delta$] or slightly increased [α_4(R135H)$\beta_1\delta$] compared with WT (Fig. 1, D–F; Supplemental Fig. 1; Supplemental Table 2; Table 1). Interestingly, only a single of the introduced mutations at α_4(F133) and α_4(G191) showed changed responses, which could not readily be explained.

As we and others have previously observed methodological limitations in the FMP assay (Wafford et al., 2009; Falk-Petersen et al., 2017), we suspected that the apparent lack of modulation could be due to sensitivity limitations. Thus, to follow up, the two mutants, α_4(F133A) and α_4(G191E), were tested using whole-cell patch-clamp electrophysiology. At both mutated receptors, DS2 modulated the GABA EC_{20}-induced currents in a concentration-dependent manner similar to WT or with even higher efficacy (Fig. 1, G and H). Each of the five δ-subunit mutations were also tested in the FMP assay. These were all functional and displayed unchanged responsiveness to DS2 compared with WT (Supplemental Fig. 2; Supplemental Tables 3 and 4).

Altogether, we conclude that the C-loop pocket in the ECD $\alpha_4^{(+)}\delta^{(-)}$ interface is not the site responsible for the PAM effect of DS2.

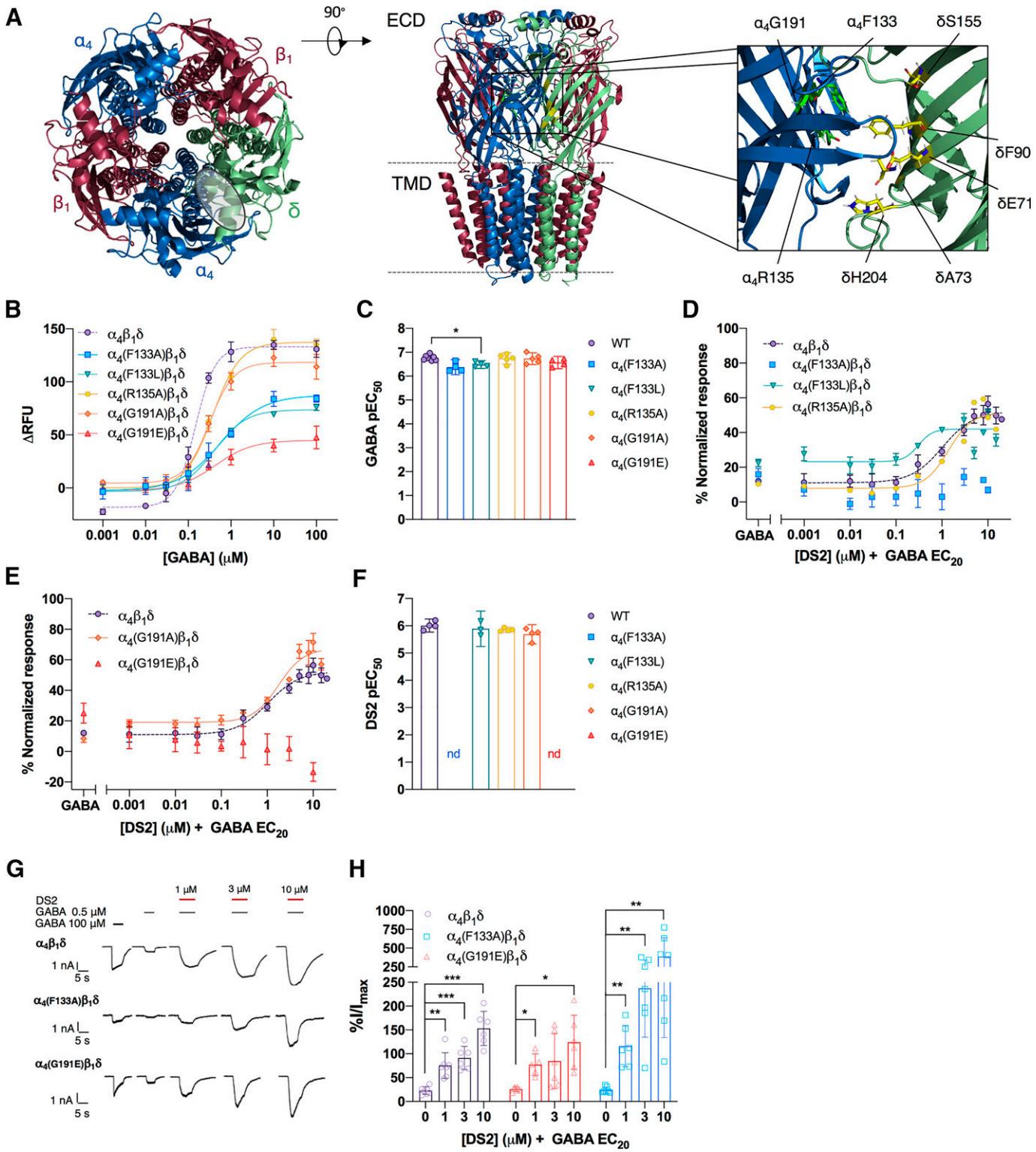

Fig. 1. Investigation of the potential ECD $\alpha_4^{(+)}\delta^{(-)}$ interface binding site. (A) Model of the $\alpha_4\beta_1\delta$ receptor with zoom in on mutated residues in the $\alpha_4^{(+)}\delta^{(-)}$ interface [built on the cryo-EM structure of $\alpha_1\beta_2\gamma_2$ (PBD code: 6D6T)]. (B) Single representative GABA concentration-response curves for α_4-mutant receptors (means ± S.D., technical triplicates) and (C) bar diagram of pooled pEC_{50} values (means with 95% confidence intervals (CI), each point representing an independent replicate (n = 4–8). (D and E) Concentration-response curves of the modulation of GABA EC_{20} by DS2 at α_4-mutant receptors (normalized means ± S.D., technical triplicates) and (F) bar diagram of pooled pEC_{50} values [means with 95% CI, each point representing an independent replicate (n = 3–5)]. (G) Single-cell representative current traces from whole-cell patch-clamp electrophysiology recordings of the modulation of GABA EC_{20} induced currents by DS2 at WT $\alpha_4\beta_1\delta$ and mutants a_4(F133A)$\beta_1\delta$ and α_4(G191E)$\beta_1\delta$ receptors. (H) Bar diagram summarizing the modulation by DS2 of α_4 mutants α_4(F133A) and α_4(G191E) cf. WT (note the broken y-axis). Currents were normalized to the maximum GABA current and presented as mean $\%I/I_{max}$ with 95% CI from minimum two independent transfections (n = 5–7). (C, F, and H) Statistical analysis was performed using two-sided Welch's t test compared with WT (C and F) or control current (H) and adjusted for multiple testing using the original FDR method of Benjamini and Hochberg with a discovery rate of 0.05. Statistical significance: $^*P < 0.05$, $^{**}P < 0.01$, $^{***}P < 0.001$.

TABLE 1
Potencies of DS2 at WT and ECD α_4-mutant receptors determined in the FMP assay.
EC_{20} is the calculated GABA concentration co-applied with the PAM. Statistical analysis is as follows: two-tailed Welch's t test compared with WT, adjusted for multiple comparison using the original FDR (Benjamini and Hochberg) method with discovery rate of 0.05.

Receptor	DS2 (PAM) EC_{50}	pEC_{50} (95% CI), n	Difference pEC_{50} [95% CI]	P Value	Adjusted P Value	GABA EC_{20}
	μM					μM
WT	0.97	6.01 (5.77;6.25), 4	—	—	—	0.06
$\alpha_{4(F133A)}\beta_1\delta$	—[a]	$n = 5$	—	—	—	0.12
$\alpha_{4(F133L)}\beta_1\delta$	1.29	5.89 (5.24;6.54), 3	−0.12 [−0.65;0.42]	0.53	0.7857	0.12
$\alpha_{4(R135A)}\beta_1\delta$	1.41	5.85 (5.76;5.95), 4	−0.15 [−0.38;0.075]	0.14	0.4500	0.06
$\alpha_{4(G191A)}\beta_1\delta$	2.04	5.69 (5.77;6.25), 4	−0.32 [−0.66;0.02]	0.061	0.3050	0.12
$\alpha_{4(G191E)}\beta_1\delta$	—[a]	$n = 5$	—	—	—	0.06

[a]Not able to fit, but a small potentiation seen for concentrations higher than 1 μM.

Identification of the TMD $\alpha_4^{(+)}\beta_1^{(-)}$ Interface as the Site of Modulation by DS2. Next, we looked into two pockets in the TMD $\alpha\beta$ interfaces (specifically involving TM2) as potential recognition sites for DS2 based on the hypothesis that diazepam and DS2 exhibit analogous binding sites in the TMD. Mutations in $\alpha_4\beta_1\delta$ TMD pockets were suggested based on the cryo-EM structure of the human $GABA_AR$ $\alpha_1\beta_3\gamma_{2L}$ (Protein Data Bank code: 6HUP) in combination with a sequence alignment due to the high (>90%) local sequence identity of the subunits within the TMD region of interest. The first pocket is located in the $\beta^{(+)}\alpha^{(-)}$ interface in a site equivalent to the recently identified low-affinity binding site for diazepam (Laverty et al., 2019).

The mutations, β_1(S290F) on the $\beta_1^{(+)}$ side and α_4(L302Y) on the $\alpha_4^{(-)}$ side, were initially probed because of an apparent central positioning of the residues in the pocket and orientation toward diazepam in the cryo-EM structure (Fig. 2A). As a similar pocket is present at the reverse subunit interface, we also included the corresponding mutations in the $\alpha_4^{(+)}\beta_1^{(-)}$ interface, α_4(S303L) on the $\alpha_4^{(+)}$ side and β_1(I289Q) on the $\beta_1^{(-)}$ side. However, as this pocket appears noticeably smaller than the $\beta_1^{(+)}\alpha_4^{(-)}$ pocket, these were mutated into more flexible and less bulky residues. Additionally, to probe both proposed pockets simultaneously, we included the double-mutant receptors α_4(L302Y,S303L)$\beta_1\delta$ and $\alpha_4\beta_1$(I289Q,S290F)δ. The introduced mutations were expected to revert hydrophilicity/hydrophobicity and introduce steric hindrance and thus would be anticipated to decrease or altogether abolish the effect of DS2.

First, we show that all the single-mutant receptors were GABA-responsive and thus functional in the FMP assay (Fig. 2B). The two β-mutants β_1(S290F) and β_1(I289Q) displayed 6.8 and 8.1 times increased GABA potencies, respectively, and the α_4(S303L)$\beta_1\delta$ mutant displayed 2.9 times increased potency compared with WT (Fig. 2C; Supplemental Table 5). Since the receptors were functional, we continued with the studies.

In the modulation experiments, we switched to DS2OMe, an analog of DS2 (L'Estrade et al., 2019) with the same pharmacological profile, because of both solubility issues with DS2 (described in the *Materials and Methods* section) and the general sensitivity limitations observed in the FMP assay on the ECD mutants. First, we examined the modulation of GABA EC_{20} at mutations introduced in the $\beta^{(+)}\alpha^{(-)}$ interface, equal to the low-affinity diazepam binding site in the γ-containing receptor (Fig. 2D). These mutations did not affect the modulation by DS2OMe, as both the $\alpha_4\beta_1$(S290F)δ and α_4(L302Y)$\beta_1\delta$ mutant receptors had DS2OMe potencies similar to WT, although a small, significant increase in efficacy for the α_4(L302Y)$\beta_1\delta$ mutant compared with WT was observed (**P = 0.0063, two-tailed Welch's t test, response of 3 μM DS2OMe) (Fig. 2, D and F; Table 2).

By contrast, when turning to the alternative $\alpha_4^{(+)}\beta_1^{(-)}$ interface, we observed significant decreases in responsiveness to modulation by DS2OMe. The α_4(S303L)$\beta_1\delta$ receptor lacked responsiveness to modulation by DS2OMe, and the β-mutant receptor $\alpha_4\beta_1$(I289Q)δ had a statistically significant 3.2 times reduction of the potency of DS2OMe compared with the WT receptor (Fig. 2, E and F; Table 2). Additionally, as expected from the individual mutations, the double-mutant receptor α_4(L302Y,S303L)$\beta_1\delta$ was not modulated by DS2OMe (Supplemental Fig. 3; Supplemental Table 6).

To verify the FMP results, we performed whole-cell patch-clamp electrophysiology recordings. Convincingly, we found no or very limited DS2 modulation of the GABA currents in the α_4(S303L)$\beta_1\delta$ and $\alpha_4\beta_1$(I289Q)δ receptor [only 10 μM modulated the $\alpha_4\beta_1$(I289Q)δ receptor by significantly increasing the GABA control current to 54.8% of the GABA I_{max}] (**P = 0.0063, two-tailed Welch's t test, adjusted, n = 5 to 6) (Fig. 2, G and H). Further, we included the double-mutant receptor α_4(S303L)β_1(I289Q)δ, which was even less modulated by 10 μM DS2, amounting to 44% of the GABA I_{max} (*P = 0.016, two-tailed Welch's t test, adjusted, n =6–9) (Fig. 2, G and H; Supplemental Tables 3 and 6). DS2OMe showed no modulation of the GABA response in either $\alpha_4\beta_1$(I289Q)δ or α_4(S303L)$\beta_1\delta$ receptors or the double-mutant α_4(S303L)β_1(I289Q)δ receptor (Supplemental Fig. 4).

Together, these results strongly advocate for the identified TMD $\alpha^{(+)}\beta^{(-)}$ interface site as the site responsible for the modulatory action of DS2.

Known $GABA_AR$ PAMs Show Unchanged Modulation at DS2-Insensitive Mutant Receptors. To confirm that the mutant receptors with altered DS2 sensitivity were not overall compromised in their general PAM responsiveness, we tested etomidate (Hill-Venning et al., 1997) and AA29504 (Hoestgaard-Jensen et al., 2010; Olander et al., 2018) at both WT and the single mutants α_4(S303L)$\beta_1\delta$ and $\alpha_4\beta_1$(I289Q)δ. In the FMP assay, both compounds showed intact positive modulation of both mutants compared with WT. Potencies (pEC_{50}) of etomidate were at WT $\alpha_4\beta_1\delta$ determined to 5.11 (EC_{50} 7.8 μM), and for the α_4(S303L)$\beta_1\delta$ and $\alpha_4\beta_1$(I289Q)δ mutants to 5.21 and 5.03 (EC_{50} 6.2 μM and 9.3 μM), respectively (Fig. 2, I and J; Table 3) (NS, two-tailed Welch's t test, n =3 to 4). Further, AA29504 showed similar

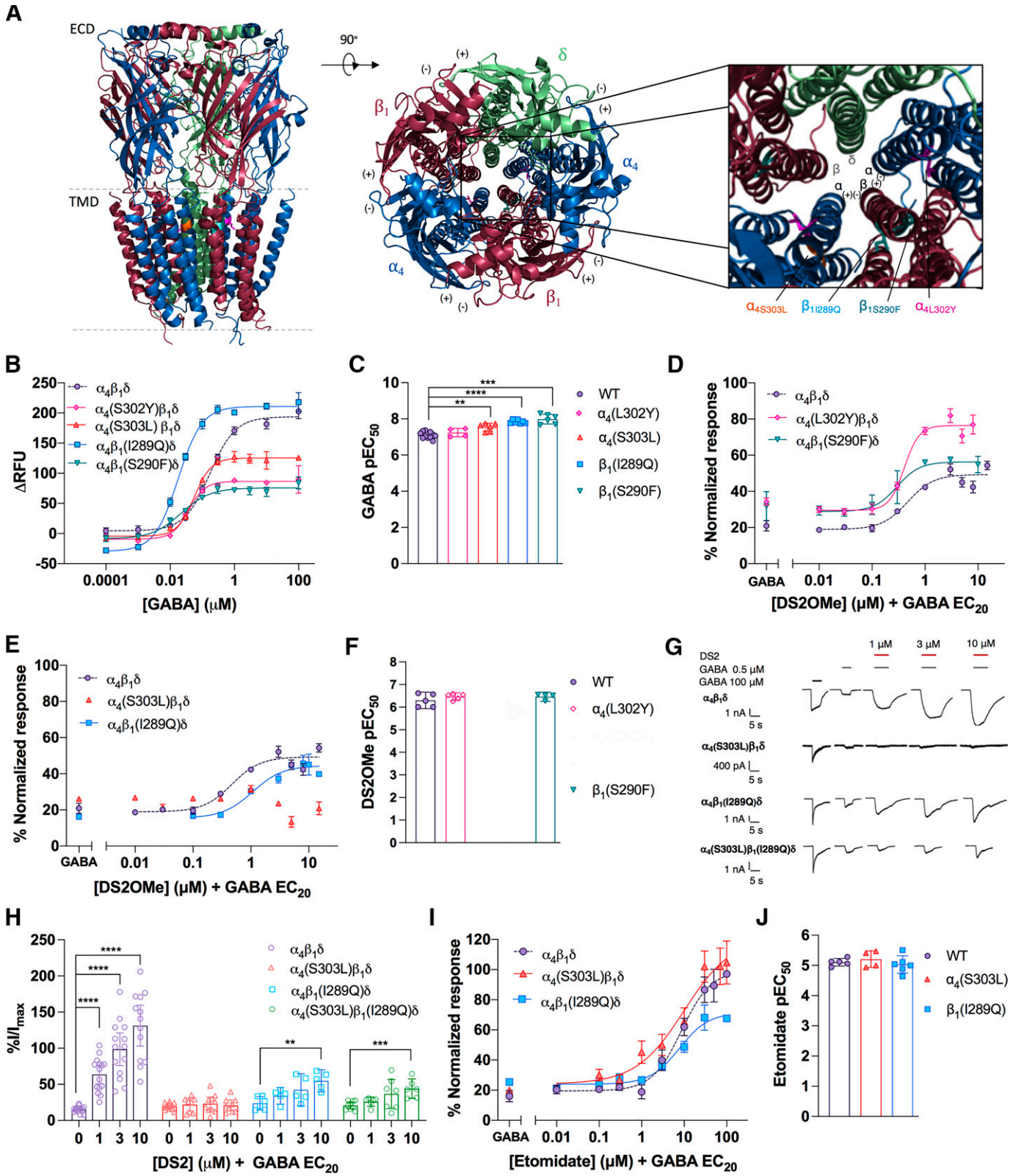

Fig. 2. Identification of the TMD $\alpha_4^{(+)}\beta_1^{(-)}$ site mediating modulation by DS2. (A) Model of the $\alpha_4\beta_1\delta$ receptor with the TMD $\beta_1^{(+)}\alpha_4^{(-)}$ and $\alpha_4^{(+)}\beta_1^{(-)}$ interface mutants highlighted in the zoomed-in image [build on the cryo-EM structure of the $\alpha_1\beta_3\gamma_2$ receptor (PBD code: 6HUP)]. (B) Single representative GABA concentration-response curves from WT $\alpha_4\beta_1\delta$ and TMD $\alpha\beta$ interface mutants (means ± S.D., technical triplicates) and (C) bar diagram showing pooled pEC_{50} values [means with 95% CI (n = 4–11)]. Modulation of GABA EC_{20} by DS2OMe (D) at the $\beta_1^{(+)}\alpha_4^{(-)}$ and (E) the $\alpha_4^{(+)}\beta_1^{(-)}$ interface mutants. Data are representative curves from a single experiment with means ± S.D. of data normalized to $GABA_{max}$. (F) Bar diagram showing pooled pEC_{50} values (means with 95% CI (n = 4–7)]. (G) Single-cell current traces from DS2 modulation of GABA EC_{20} at WT and $\alpha_4^{(+)}\beta_1^{(-)}$ interface mutants. (H) Bar diagram summarizing the DS2 modulation of $\alpha_4^{(+)}\beta_1^{(-)}$ interface single and double mutants in whole-cell patch-clamp electrophysiology. Currents are normalized to the $GABA_{max}$ current and are given as mean $\%I/I_{max}$ with 95% CI

TABLE 2
Potencies of DS2OMe at TMD mutant receptors determined in the FMP assay.
EC_{20} is the calculated GABA concentration co-applied with the PAM. Statistical analysis is as follows: two-tailed Welch's t test compared with WT, adjusted for multiple comparison using the original FDR (Benjamini and Hochberg) method with discovery rate of 0.05.

Receptor	DS2OMe (PAM) EC_{50}	DS2OMe (PAM) pEC_{50} (95% CI), n	Difference pEC_{50} [95% CI]	P Value	Adjusted P Value	GABA EC_{20}
	μM					μM
WT	0.50	6.30 (5.9;6.7), 5	—	—	—	0.03
$\alpha_{4(L302Y)}\beta_1\delta$	0.35	6.46 (6.3;6.6), 5	0.17 [−0.19;0.52]	0.29	0.310	0.044
$\alpha_{4(S303L)}\beta_1\delta$	—	$n = 3^a$	—	—	—	0.023
$\alpha_4\beta_{1(I289Q)}\delta$	1.58	5.80 (5.6;6.0), 7	−0.49 [−0.85;−0.12]	0.015	0.045*	0.005
$\alpha_4\beta_{1(S290F)}\delta$	0.35	6.46 (6.3;6.7), 4	0.16 [−0.20;0.52]	0.31	0.310	0.03

[a]No apparent potentiation (concentration range from 0.01 μM to 10 μM DS2OMe).
*$P < 0.05$.

potentiation at the mutants and WT receptors (Supplemental Fig. 5; Supplemental Table 7), indicating that it does not mediate its effect through the same site as DS2, correlating with a proposed binding site for AA29504 in the TMD $\beta^{(+)}\alpha^{(-)}$ interface (Olander et al., 2018).

Induced-Fit Docking of DS2 and DS2OMe Corroborates Mutational Results. Guided by the mutational data confirming the molecular recognition site mediating the effect of DS2 and DS2OMe in the transmembrane part of the $\alpha_4{}^{(+)}\beta_1{}^{(-)}$-subunit interface, we constructed a model of the modulator-receptor binding mode. Based on the structure of the desensitized $\alpha_1\beta_3\gamma_{2L}$ receptor bound to GABA and diazepam (Masiulis et al., 2019), we constructed a homology model of the $\alpha_4\beta_1$-subunit interface into which DS2 and DS2OMe were fitted using induced-fit docking. Allowing residue side chains in the "empty" homology model to adapt to the modulators, we obtained very similar binding modes for the docked compounds (Fig. 3; Supplemental Fig. 5). The core scaffold binds with the amide carbonyl of DS2 showing a potential hydrogen bond to the hydroxy group of Ser303 in α_4. Using a backbone-dependent rotamer library, we observe that the α_4(S303L) mutation removes the hydrogen bond and sterically blocks the binding site, providing an explanation for the observed lack of potentiation on this mutant (Fig. 3B). Ile289 in β_1 lines 4-fluorophenyl of DS2, contributing to the binding through substantial van der Waal contacts, and the I289Q mutation has a steric clash with DS2 (Fig. 3B). As for the α_4(S303L) mutant, these effects provide a possible explanation for the observed abolishment of potentiation at all but the highest concentration of DS2 and DS2OMe in our patch-clamp experiments, and the obtained binding mode thus concurs with the experimental results. Our previously published analogs of DS2 show that there should be room for much larger substituents than the methoxy of DS2OMe as well as a bromo atom in the 5-position on the imidazol[1,2-a] pyridine scaffold (Rostrup et al., 2021). Thus, we provide further proof of concept for the predicted binding site by docking the recently published analog, Br-DS2OPh (Rostrup et al., 2021). This confirmed that the OPh substituent can fit the binding site in the homology model with only a minor shift in the binding mode (Supplemental Fig. 5).

Discussion

From our experiments using systematic structural iterations and experimental validation of known and proposed binding sites, we here present the elusive DS2 interaction site as a distinct site encompassing α_4S303 and β_1I289 residues in the TMD $\alpha_4{}^{(+)}\beta_1{}^{(-)}$ interface of $\alpha_4\beta_1\delta$ receptors. This novel site is similar in nature both to the low-affinity diazepam binding site identified in the cryo-EM structure of the $\alpha_1\beta_3\gamma_2$ receptor (Laverty et al., 2019) and the site for general anesthetics (e.g., etomidate) (Li et al., 2006) and the proposed binding site for AA29504 (Olander et al., 2018). Notably, the residues in the new DS2 site are located on the alternative intersubunit interface $\alpha_4{}^{(+)}\beta_1{}^{(-)}$, explaining why our mutations do not affect etomidate or AA29504 PAM activity. Indeed, it has been reported that pockets exist in all the TMD intersubunit interfaces (Sieghart et al., 2012; Forman and Miller, 2016; Iorio et al., 2020) and that several known

TABLE 3
Potency of etomidate at $\alpha_4{}^{(+)}\beta_1{}^{(-)}$ TMD mutants determined in the FMP assay.
EC_{20} is the calculated GABA concentration co-applied with the PAM. Statistical analysis is as follows: two-tailed Welch's t test compared with WT, and adjusted for multiple testing using the original FDR (Benjamini and Hochberg) method with discovery rate of 0.05.

Receptor	Etomidate (PAM) EC_{50}	pEC_{50} (95% CI), n	Difference pEC_{50} [95% CI]	P Value	Adjusted P Value	GABA EC_{20}
	μM					μM
WT	7.8	5.11 (5.1;7.4), 5	—	—	—	0.06
$\alpha_{4(S303L)}\beta_1\delta$	6.2	5.21 (6.0;7.2), 4	−0.10 [−1.3;0.60]	0.36	0.66	0.02
$\alpha_4\beta_{1(I289Q)}\delta$	9.3	5.03 (6.1;6.2), 5	−0.07 [−1.42;1.31]	0.66	0.66	0.007

(n = 5–16). (I) Single representative concentration-response curves of the modulation of GABA EC_{20} by etomidate at the $\alpha_4{}^{(+)}\beta_1{}^{(-)}$ interface mutants and (J) pooled pEC_{50} values [means with 95% CI, with symbols representing values from independent experiments (n = 4 to 5)]. (C, F, H, and J) Statistical analysis was performed using two-sided Welch's t test compared with WT (C, F, and J) or control current (H) and adjusted for multiple testing using the original FDR method of Benjamini and Hochberg with a discovery rate of 0.05. Statistical significance: *$P < 0.05$, **$P < 0.01$, ***$P < 0.001$, and ****$P < 0.0001$.

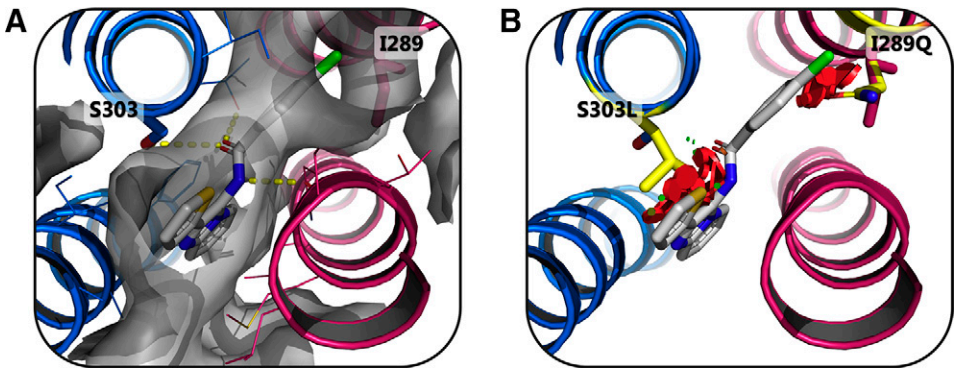

Fig. 3. Binding model of DS2 in the TMD $\alpha_4^{(+)}\beta_1^{(-)}$-subunit interface. Visualization of DS2 (sticks and gray carbon atoms) in the TMD interface between the α_4 (blue cartoon and carbon atoms) and β_1 (magenta cartoon and carbon atoms) $GABA_A$ subunits, showing: (A) Residues with side chain atoms within 5 Å of DS2 are shown as lines highlighting the two important residues, α_4S303 and β_1I289, as sticks. The binding cavity is depicted as the vdW surface (gray and transparent) of the same residues and hydrogen bonds between DS2 and the receptor represented as yellow dotted lines. (B) *In silico* representation of the α_4S303L and β_1I289Q mutations (inserted residues as sticks with yellow carbon atoms) showing predicted steric clashes with DS2 as red disks explaining the hampered/abolished positive modulation of DS with these mutations. Figure prepared with the PyMOL Molecular Graphics System, Version 2.0 Schrödinger, LLC.

allosteric modulators can bind in these pockets (Olsen, 2018). This shows how different $GABA_A$ receptors subtypes have evolved to include different functionally relevant allosteric sites.

The $\alpha_4\beta_1\delta$ subtype was selected as model receptor in this study because of previous success with this for detailed and reliable molecular pharmacology examination (Falk-Petersen et al., 2017, 2020; Dalby et al., 2020). The expression of the δ-subunit relies on an in-house–generated stable δ-HEK cell line and subsequent transfection with α- and β-subunits of choice, including mutated subunits, to generate functional $\alpha\beta\delta$ receptors that can be evaluated via measurements of membrane potential changes by fluorescence in the medium-throughput FMP assay (Falk-Petersen et al., 2017). The combination of α_4- and β_1-subunits was selected because α_4 is often encountered together with δ in native receptors (Lee and Maguire, 2014) and because β_1 conveniently does not lead to the formation of homomeric receptors in this system (Falk-Petersen et al., 2017). Indeed, using this setup, we here demonstrate the measurement of both reliable GABA responses and various PAM effects at $\alpha_4\beta_1\delta$ receptors. We also report the successful generation of several stable δ-mutant cell lines, thus underlining this expression system as a versatile methodological tool for studying δ-$GABA_A$ molecular pharmacology in HEK cells with low variability. In cases of low-expressing receptors, as seen with some of the mutants examined here, we observed some discrepancies in the data obtained between FMP and patch-clamp electrophysiology. In this case, the FMP assay, which measures overall changes in membrane potential, appears to have some limitations as a result of lower overall sensitivity, especially in relation to efficacy of low-expressing mutants.

In our path to identifying the DS2 TMD interface binding site, we first examined one of the usual suspects, the ECD intersubunit $\alpha_4^{(+)}\delta^{(-)}$ interface, or the C-loop pocket (Jensen et al., 2013; Masiulis et al., 2019), as the site responsible for the PAM effect of DS2. Although the existence of this pocket has previously been debated (Wafford et al., 2009; Jensen et al., 2013; Ahring et al., 2016), we included it because of an observed structural resemblance between DS2 and the benzodiazepine binding site ligand zolpidem, which could suggest a potentially shared benzodiazepine-like binding site. We can now refute this hypothesis, also corroborated by our recent structure-activity relationship study of DS2 analogs targeting this site (Rostrup et al., 2021). Incidentally, one of these analogs (Br-DS2OPh), designed to bind in the ECD $\alpha^{(+)}$-$\delta^{(-)}$ interface, fits well into the identified DS2 TMD pocket in the $\alpha_4^{(+)}\beta_1^{(-)}$ interface, showing the importance of experimental validation of binding site hypotheses based on molecular modeling. This further identifies Br-DS2OPh as a useful DS2 analog for future studies.

From our data, it is evident that the δ-subunit is not directly involved in the modulation by DS2, questioning what determines the δ-selective profile of the compounds. This is in accordance with previous data by Yakoub et al. (2018), who found that DS2 is capable of modulating receptors (in particular binary $\alpha_6\beta_3$ receptors) that do not contain a δ-subunit. It is plausible that this is a matter of functional selectivity, similar to that observed for the superagonist 4,5,6,7-Tetrahydroisoxazolo[5,4-c]pyridin-3-ol hydrochloride (THIP) (gaboxadol), in which case binding in a highly conserved α-β interface gives rise to 10 times higher potency at the δ-containing receptors compared with both γ-containing and binary $\alpha\beta$ receptors (Stórustovu and Ebert, 2006; Mortensen et al., 2010; Falk-Petersen et al., 2017). Also, PAMs (such as neurosteroids) have been found to display functional selectively at δ-containing receptors (Stell et al., 2003; Ahring et al., 2016), supposedly because GABA itself is only a partial agonist, leaving room for further activation (Dalby et al., 2020). Now, having a homology model of the confirmed DS2 binding site, the next step is to use this for structure-based drug design of DS2-related analogs or a radiolabeled analog for further validation of the binding site. Already, we have shown that classic medicinal chemistry approaches can improve both potency and selectivity of DS2 (Rostrup et al., 2021) and potentially brain permeability (L'Estrade et al., 2019). However, in line with already reported PAM effects, DS2's functional activity is most effective at δ-containing subtypes (Jensen et al., 2013; Ahring et al., 2016; Yakoub et al., 2018) as a result of yet unknown factors. Ultimately, a cryo-EM structure in complex with one of the DS2 analogs would map the binding pocket including additional molecular interaction points and discern potential differences among subtypes.

In conclusion, our identification of the long-sought-after DS2 interaction site in the $\alpha_4\beta_1\delta$ receptor may promote new insights into this highly important drug target class of

δ-containing receptors suffering a general lack of selective tool compounds. Novel δ-selective analogs will aid to improve our understanding of the physiologic and pathophysiological role of δ-containing receptors. Such compounds may therefore potentially serve as leads for future rational drug development to treat the vast majority of neurologic disorders with dysregulated tonic inhibition as well as targeting conditions involving δ-containing $GABA_A$ receptors in the periphery, such as inflammation and immune disorders.

Acknowledgments

We would like to thank Dr. Uffe Kristiansen for intellectual input and scientific guidance with the patch-clamp electrophysiology studies and Durita Poulsen for technical assistance.

Authorship Contributions

Participated in research design: Falk-Petersen, Rostrup, Harpsøe, Gloriam, Frølund, Wellendorph.

Conducted experiments: Falk-Petersen, Rostrup, Löffler, Buchleithner, Harpsøe.

Contributed new reagents or analytic tools: Rostrup, Frølund.

Performed data analysis: Falk-Petersen, Rostrup, Löffler, Buchleithner, Harpsøe, Wellendorph.

Wrote or contributed to the writing of the manuscript: Falk-Petersen, Harpsøe, Wellendorph.

References

Ahring PK, Bang LH, Jensen ML, Strøbæk D, Hartiadi LY, Chebib M, and Absalom N (2016) A pharmacological assessment of agonists and modulators at $\alpha_4\beta_2\gamma_2$ and $\alpha_4\beta_2\delta$ $GABA_A$ receptors: The challenge in comparing apples with oranges. *Pharmacol Res* **111**:563–576.

Barrera NP, Betts J, You H, Henderson RM, Martin IL, Dunn SM, and Edwardson JM (2008) Atomic force microscopy reveals the stoichiometry and subunit arrangement of the α4β3δ GABA(A) receptor. *Mol Pharmacol* **73**:960–967.

Baumann SW, Baur R, and Sigel E (2002) Forced subunit assembly in α1β2γ2 GABAA receptors. Insight into the absolute arrangement. *J Biol Chem* **277**:46020–46025.

Baur R, Kaur KH, and Sigel E (2009) Structure of α_6 β_3 δ $GABA_{(A)}$ receptors and their lack of ethanol sensitivity. *J Neurochem* **111**:1172–1181.

Belelli D, Harrison NL, Maguire J, Macdonald RL, Walker MC, and Cope DW (2009) Extrasynaptic $GABA_A$ receptors: form, pharmacology, and function. *J Neurosci* **29**:12757–12763.

Clarkson AN, Huang BS, Macisaac SE, Mody I, and Carmichael ST (2010) Reducing excessive GABA-mediated tonic inhibition promotes functional recovery after stroke. *Nature* **468**:305–309.

Cope DW, Di Giovanni G, Fyson SJ, Orbán G, Errington AC, Lorincz ML, Gould TM, Carter DA, and Crunelli V (2009) Enhanced tonic $GABA_A$ inhibition in typical absence epilepsy. *Nat Med* **15**:1392–1398.

Dalby NO, Falk-Petersen CB, Leurs U, Scholze P, Krall J, Frølund B, and Wellendorph P (2020) Silencing of spontaneous activity at α4β1/3δ $GABA_A$ receptors in hippocampal granule cells reveals different ligand pharmacology. *Br J Pharmacol* **177**:3975–3990.

Ernst M, Bruckner S, Boresch S, and Sieghart W (2005) Comparative models of $GABA_A$ receptor extracellular and transmembrane domains: important insights in pharmacology and function. *Mol Pharmacol* **68**:1291–1300.

Falk-Petersen CB, Søgaard R, Madsen KL, Klein AB, Frølund B, and Wellendorph P (2017) Development of a robust mammalian cell-based assay for studying recombinant $\alpha_4\beta_{1/3}\delta$ $GABA_A$ receptor subtypes. *Basic Clin Pharmacol Toxicol* **121**:119–129.

Falk-Petersen CB, Tsonkov TM, Nielsen MS, Harpsøe K, Bundgaard C, Frølund B, Kristiansen U, Gloriam DE, and Wellendorph P (2020) Discovery of a new class of orthosteric antagonists with nanomolar potency at extrasynaptic $GABA_A$ receptors. *Sci Rep* **10**:10078.

Farrant M and Nusser Z (2005) Variations on an inhibitory theme: phasic and tonic activation of $GABA_{(A)}$ receptors. *Nat Rev Neurosci* **6**:215–229.

Forman SA and Miller KW (2016) Mapping general anesthetic sites in heteromeric γ-aminobutyric acid type A receptors reveals a potential for targeting receptor subtypes. *Anesth Analg* **123**:1263–1273.

Hill-Venning C, Belelli D, Peters JA, and Lambert JJ (1997) Subunit-dependent interaction of the general anaesthetic etomidate with the gamma-aminobutyric acid type A receptor. *Br J Pharmacol* **120**:749–756.

Hoestgaard-Jensen K, Dalby NO, Wolinsky TD, Murphey C, Jones KA, Rottländer M, Frederiksen K, Watson WP, Jensen K, and Ebert B (2010) Pharmacological characterization of a novel positive modulator at $\alpha_4\beta_3$ δ-containing extrasynaptic $GABA_{(A)}$ receptors. *Neuropharmacology* **58**:702–711.

Iorio MT, Vogel FD, Koniuszewski F, Scholze P, Rehman S, Simeone X, Schnürch M, Mihovilovic MD, and Ernst M (2020) $GABA_A$ receptor ligands often interact with binding sites in the transmembrane domain and in the extracellular domain-can the promiscuity code be cracked? *Int J Mol Sci* **21**:334.

Jensen ML, Wafford KA, Brown AR, Belelli D, Lambert JJ, and Mirza NR (2013) A study of subunit selectivity, mechanism and site of action of the delta selective compound 2 (DS2) at human recombinant and rodent native $GABA_{(A)}$ receptors. *Br J Pharmacol* **168**:1118–1132.

Karim N, Wellendorph P, Absalom N, Bang LH, Jensen ML, Hansen MM, Lee HJ, Johnston GAR, Hanrahan JR, and Chebib M (2012) Low nanomolar GABA effects at extrasynaptic α4β1/β3δ GABA(A) receptor subtypes indicate a different binding mode for GABA at these receptors. *Biochem Pharmacol* **84**:549–557.

Kaur KH, Baur R, and Sigel E (2009) Unanticipated structural and functional properties of δ-subunit-containing $GABA_A$ receptors. *J Biol Chem* **284**:7889–7896.

Kim S, Chen J, Cheng T, Gindulyte A, He J, He S, Li Q, Shoemaker BA, Thiessen PA, Yu B et al. (2019) PubChem 2019 update: improved access to chemical data. *Nucleic Acids Res* **47** (D1):D1102–D1109.

L'Estrade ET, Hansen HD, Falk-Petersen C, Haugaard A, Griem-Krey N, Jung S, Lüddens H, Schirmeister T, Erlandsson M, Ohlsson T, et al. (2019) Synthesis and pharmacological evaluation of $[^{11}C]$4-methoxy-N-[2-(thiophen-2-yl)imidazo[1,2- a] pyridin-3-yl]benzamide as a brain penetrant PET ligand selective for the δ-subunit-containing γ-aminobutyric acid type A receptors. *ACS Omega* **4**:8846–8851.

Laverty D, Desai R, Uchański T, Masiulis S, Stec WJ, Malinauskas T, Zivanov J, Pardon E, Steyaert J, Miller KW, et al. (2019) Cryo-EM structure of the human $\alpha1\beta3\gamma2$ $GABA_A$ receptor in a lipid bilayer. *Nature* **565**:516–520.

Lee V and Maguire J (2014) The impact of tonic $GABA_A$ receptor-mediated inhibition on neuronal excitability varies across brain region and cell type. *Front Neural Circuits* **8**:3.

Li GD, Chiara DC, Sawyer GW, Husain SS, Olsen RW, and Cohen JB (2006) Identification of a $GABA_A$ receptor anesthetic binding site at subunit interfaces by photolabeling with an etomidate analog. *J Neurosci* **26**:11599–11605.

Lie MEK, Gowing EK, Johansen NB, Dalby NO, Thiesen L, Wellendorph P, and Clarkson AN (2019) GAT3 selective substrate l-isoserine upregulates GAT3 expression and increases functional recovery after a focal ischemic stroke in mice. *J Cereb Blood Flow Metab* **39**:74–88.

Masiulis S, Desai R, Uchański T, Serna Martin I, Laverty D, Karia D, Malinauskas T, Zivanov J, Pardon E, Kotecha A, et al. (2019) $GABA_A$ receptor signalling mechanisms revealed by structural pharmacology. *Nature* **565**:454–459.

Michel MC, Murphy TJ, and Motulsky HJ (2020) New author guidelines for displaying data and reporting data analysis and statistical methods in experimental biology. *Mol Pharmacol* **97**:49–60.

Mody I (2001) Distinguishing between $GABA_{(A)}$ receptors responsible for tonic and phasic conductances. *Neurochem Res* **26**:907–913.

Mortensen M, Ebert B, Wafford K, and Smart TG (2010) Distinct activities of GABA agonists at synaptic- and extrasynaptic-type $GABA_A$ receptors. *J Physiol* **588**:1251–1268.

Neumann S, Boothman-Burrell L, Gowing EK, Jacobsen TA, Ahring PK, Young SL, Sandager-Nielsen K, and Clarkson AN (2019) The delta-subunit selective $GABA_A$ receptor modulator, DS2, improves stroke recovery via an anti-inflammatory mechanism. *Front Neurosci* **13**:1133.

Olander ER, Madjroh N, Bunch L, Söderhielm PC, and Jensen AA (2018) Delineation of the functional properties and the mechanism of action of AA29504, an allosteric agonist and positive allosteric modulator of $GABA_A$ receptors. *Biochem Pharmacol* **150**:305–319.

Olsen RW (2018) $GABA_A$ receptor: positive and negative allosteric modulators. *Neuropharmacology* **136** (Pt A):10–22.

Olsen RW and Sieghart W (2009) $GABA_A$ receptors: subtypes provide diversity of function and pharmacology. *Neuropharmacology* **56**:141–148.

Patel B, Mortensen M, and Smart TG (2014) Stoichiometry of δ subunit containing $GABA_{(A)}$ receptors. *Br J Pharmacol* **171**:985–994.

Puthenkalam R, Hieckel M, Simeone X, Suwattanasophon C, Feldbauer RV, Ecker GF, and Ernst M (2016) Structural studies of $GABA_A$ receptor binding sites: which experimental structure tells us what? *Front Mol Neurosci* **9**:44.

Rostrup F, Falk-Petersen CB, Harpsø E K, Buchleithner S, Conforti I, Jung S, Gloriam DE, Schirmeister T, Wellendorph P, and Frø Lund B (2021) Structural determinants for the mode of action of the imidazopyridine DS2 at δ-containing γ-aminobutyric acid type A ($GABA_A$) receptors. *J Med Chem* **64**:4730–4743.

Sastry GM, Adzhigirey M, Day T, Annabhimoju R, and Sherman W (2013) Protein and ligand preparation: parameters, protocols, and influence on virtual screening enrichments. *J Comput Aided Mol Des* **27**:221–234.

Sieghart W, Ramerstorfer J, Sarto-Jackson I, Varagic Z, and Ernst M (2012) A novel $GABA_{(A)}$ receptor pharmacology: drugs interacting with the α(+) β(-) interface. *Br J Pharmacol* **166**:476–485.

Sigel E and Steinmann ME (2012) Structure, function, and modulation of $GABA_{(A)}$ receptors. *J Biol Chem* **287**:40224–40231.

Simeone X, Iorio MT, Siebert DCB, Rehman S, Schnürch M, Mihovilovic MD, and Ernst M (2019) Defined concatenated $\alpha6\alpha1\beta3\gamma2$ $GABA_A$ receptor constructs reveal dual action of pyrazoloquinolinone allosteric modulators. *Bioorg Med Chem* **27**:3167–3178.

Stell BM, Brickley SG, Tang CY, Farrant M, and Mody I (2003) Neuroactive steroids reduce neuronal excitability by selectively enhancing tonic inhibition mediated by delta subunit-containing GABAA receptors. *Proc Natl Acad Sci USA* **100**:14439–14444.

Stórustovu SI and Ebert B (2006) Pharmacological characterization of agonists at δ-containing GABAA receptors: functional selectivity for extrasynaptic receptors is dependent on the absence of γ2. *J Pharmacol Exp Ther* **316**:1351–1359.

Tretter V, Ehya N, Fuchs K, and Sieghart W (1997) Stoichiometry and assembly of a recombinant $GABA_A$ receptor subtype. *J Neurosci* **17**:2728–2737.

UniProt Consortium (2019) UniProt: a worldwide hub of protein knowledge. *Nucleic Acids Res* **47** (D1):D506–D515.

Wafford KA and Ebert B (2006) Gaboxadol–a new awakening in sleep. *Curr Opin Pharmacol* **6**:30–36.

Wafford KA, van Niel MB, Ma QP, Horridge E, Herd MB, Peden DR, Belelli D, and Lambert JJ (2009) Novel compounds selectively enhance δ subunit containing $GABA_A$ receptors and increase tonic currents in thalamus. *Neuropharmacology* **56**:182–189.

Wagoner KR and Czajkowski C (2010) Stoichiometry of expressed $\alpha_{(4)}\beta_{(2)}\delta$ γ-aminobutyric acid type A receptors depends on the ratio of subunit cDNA transfected. *J Biol Chem* **285**:14187–14194.

Webb B, and Sali A (2016) Comparative protein structure modeling using MODELLER. *Curr Protoc Bioinforma* **54**:5.6.1–5.6.37.

Wongsamitkul N, Baur R, and Sigel E (2016) Toward understanding functional properties and subunit arrangement of $\alpha_4\beta_2\delta$ γ-aminobutyric Acid, Type A ($GABA_A$) receptors. *J Biol Chem* **291**:18474–18483.

Yakoub K, Jung S, Sattler C, Damerow H, Weber J, Kretzschmann A, Cankaya AS, Piel M, Rösch F, Haugaard AS, et al. (2018) Structure-function evaluation of imidazopyridine derivatives selective for δ-subunit-containing γ-aminobutyric acid type A ($GABA_A$) receptors. *J Med Chem* **61**:1951–1968.

Yocum GT, Turner DL, Danielsson J, Barajas MB, Zhang Y, Xu D, Harrison NL, Homanics GE, Farber DL, and Emala CW (2017) $GABA_A$ receptor α_4-subunit knockout enhances lung inflammation and airway reactivity in a murine asthma model. *Am J Physiol Lung Cell Mol Physiol* **313**:L406–L415.

Zhang N, Peng Z, Tong X, Lindemeyer AK, Cetina Y, Huang CS, Olsen RW, Otis TS, and Houser CR (2017) Decreased surface expression of the δ subunit of the $GABA_A$ receptor contributes to reduced tonic inhibition in dentate granule cells in a mouse model of fragile X syndrome. *Exp Neurol* **297**:168–178.

Zhu S, Noviello CM, Teng J, Walsh Jr RM, Kim JJ, and Hibbs RE (2018) Structure of a human synaptic $GABA_A$ receptor. *Nature* **559**:67–72.

Address correspondence to: Petrine Wellendorph, Universitetsparken 2, DK-2100 Copenhagen, Denmark. E-mail: pw@sund.ku.dk